Cell PRESS
Open ACCESS

Cell Reports
Report

Imaging Type VI Secretion-Mediated Bacterial Killing

Yannick R. Brunet,[1] Leon Espinosa,[2] Seddik Harchouni,[1] Tâm Mignot,[2] and Eric Cascales[1,*]
[1]Laboratoire d'Ingénierie des Systèmes Macromoléculaires (LISM, UMR 7255)
[2]Laboratoire de Chimie Bactérienne (LCB, UMR 7283)
Centre National de la Recherche Scientifique (CNRS)-Aix-Marseille University, Institut de Microbiologie de la Méditerranée (IMM), 31 chemin Joseph Aiguier, 13402 Marseille Cedex 20, France
*Correspondence: cascales@imm.cnrs.fr
http://dx.doi.org/10.1016/j.celrep.2012.11.027

SUMMARY

In the environment, bacteria compete with each other for nutrient availability or to extend their ecological niche. The type VI secretion system contributes to bacterial competition by the translocation of antibacterial effectors from predators into prey cells. The T6SS assembles a dynamic structure—the sheath—wrapped around a tube constituted of the Hcp protein. It has been proposed that by cycling between extended and contracted conformations the sheath acts as a crossbow to propel the Hcp tube toward the target cell. While the sheath dynamics have been studied in monocultures, the activity of the T6SS has not been recorded in presence of the prey. Here, time-lapse fluorescence microscopy of cocultures demonstrates that prey cells are killed upon contact with predator cells. Additional experiments provide evidence that sheath contraction correlates with nearby cell fading and that prey lysis occurs within minutes after sheath contraction. The results support a model in which T6SS dynamics are responsible for T6SS effectors translocation into recipient cells.

INTRODUCTION

In their natural habitats, bacterial species compete for the available nutrients to colonize or extend their niches or to benefit from host cells. However, it is only recently that studies have been conducted to understand how competing bacteria contribute to the growth, the fitness, and the ability to form biofilms and the regulation of virulence factors of a bacterium in mixed cultures (Sperandio, 2012). For example, commensals from the gut microbiota enable mice to eradicate the rodent pathogen *Citrobacter rodentium* upon infection (Kamada et al., 2012). In this process, commensals outcompete *C. rodentium* by utilizing the same carbon sources, limiting its growth and allowing its clearance from the digestive tract. Nutrient availability and diet are therefore important factors steering the outcome of a competition between bacteria. Recently, the type VI secretion system (T6SS) has been identified as a key player during bacterial competition between Gram-negative bacteria (Hood et al., 2010; Jani and Cotter, 2010). Secretion systems are *trans*-envelope complexes dedicated to the translocation of bacterial toxin proteins. Interestingly, the T6SS is a versatile nanomachine as it delivers protein effectors into either eukaryotic or prokaryotic target cells (Cascales, 2008; Schwarz et al., 2010b; Silverman et al., 2012). T6SS can therefore play a direct role in pathogenesis, such as in the case of *Vibrio cholerae*, through the release of toxins responsible for actin crosslinking into eukaryotic host cells (Pukatzki et al., 2007; Ma et al., 2009; Durand et al., 2012), or an indirect role through competition with neighboring bacteria (Hood et al., 2010; Schwarz et al., 2010a; MacIntyre et al., 2010; Murdoch et al., 2011; Gueguen and Cascales, 2013). To date, a few translocated antibacterial effectors have been identified and characterized. In *Pseudomonas aeruginosa*, the Tse1 and Tse3 proteins are delivered into the periplasm of prey cells where they cause lysis by deteriorating the peptidoglycan layer (Russell et al., 2011). Predator bacteria are rendered immune by the production of specific Tse-inhibiting proteins that prevent the action of the toxin (Russell et al., 2011). The toxin delivery process is achieved by a mechanism resembling DNA injection by contractile tailed bacteriophages. Basically, the bacterium builds a macromolecular complex composed of 13 Tss (Type six subunits) core components that spans the cell envelope (Cascales, 2008; Silverman et al., 2012; Cascales and Cambillau, 2012). The extracellular portion of the T6SS is composed of two proteins, Hcp and VgrG, that share structural homologies with the tail and the puncturing device of bacteriophage T4 (Mougous et al., 2006; Pell et al., 2009; Kanamaru et al., 2002; Leiman et al., 2009). In contractile bacteriophages, the tail tube is surrounded by the sheath. Upon infection, the phage sheath undergoes an extensive structural transition leading to its contraction and propels the tail tube toward the target cell interior (Leiman et al., 2004). Recently, Basler et al. (2012) showed that two core components, TssB (VipA) and TssC (VipB), assemble large tubular structures into the cytoplasm that exhibit cogwheel-like cross-sections resembling the bacteriophage sheath. Time-lapse fluorescence microscopy further demonstrated these structures as highly dynamic, oscillating between extended and contracted conformations (Basler et al., 2012). Based on the homology with the bacteriophage, it is thought that contraction of the T6SS TssB/C tubule acts as a crossbow to propel the Hcp tube toward the exterior and thus the target cell. More recently, Basler and Mekalanos

Table 1. Growth Competition between *E. coli* Strains

Prey	Predator	Fluorescence[a]	Survival[b]
None	EAEC	12,706 ± 1,304	—
W3110*gfp*$^+$	W3110	67,524 ± 5,876 (100%)	100
W3110*gfp*$^+$	EAEC	17,450 ± 2,228 (8.6%)	3.5
W3110*gfp*$^+$	EAEC Δ*clpV1*	20,265 ± 3,107 (13.7%)	6.2
W3110*gfp*$^+$	EAEC Δ*clpV2*	63,493 ± 6,014 (92.3%)	92.1

[a]Fluorescence levels relative to the optical density (in arbitrary units). The percentage is calculated as the level of fluorescence of the sample (subtracted by the background, i.e., the fluorescence of the nonfluorescent EAEC) divided by the level of fluorescence of the fluorescent strain in competition with W3110 (subtracted by the background).
[b]Survival in percentage of colony forming units (cfu) relative to the cfu of the fluorescent strain in competition with W3110.

reported that in a *P. aeruginosa* lawn, T6SS sheath contraction induces a response in neighboring immune bacteria, which then deployed a series of extension/contraction cycles (Basler and Mekalanos, 2012). This phenomenon, named dueling, may constitute a response to the stress engendered by local membrane alterations by adjacent bacteria. In all these recent studies, T6SS dynamics has been followed in pure culture, allowing characterization of the extension/contraction process and observation of bacterial dueling. However, that contraction of the T6SS sheath causes intoxication of neighboring nonimmune bacteria remains to be proved. We therefore sought to determine whether the contraction of the T6SS sheath is directly associated with target cell lysis. Here, we first show that the Sci-2 T6SS provides a growth advantage to a pathogenic strain of *Escherichia coli* in mixed culture with a laboratory, nonpathogenic strain of *E. coli*. Using time-lapse fluorescence microscopy, we then quantitatively show that the contraction of the sheath structure correlates with target cell outburst.

RESULTS AND DISCUSSION

In this study, we used the enteroaggregative *E. coli* (EAEC) strain 17-2 as a model. This pathovar of *E. coli* is an inhabitant of the digestive track of humans and causes severe and persistent diarrhea (Kaper et al., 2004). This strain carries two gene clusters encoding functional T6SS, Sci-1 and Sci-2. The Sci-1 T6SS is required for efficient biofilm formation (Aschtgen et al., 2008). We first performed a growth competition assay between EAEC and a nonpathogenic strain of *E. coli*, W3110, devoid of T6SS genes. Control experiments demonstrated that EAEC and W3110 strains share similar growth behaviors and similar generation times in pure culture. Both strains were mixed, spotted on nutritive agar plates, and incubated for 14 hr. Recovered EAEC and W3110 cells were counted on selective plates. Table 1 shows that, in mixed cultures, W3110 was killed by EAEC as the output of W3110 cells was reduced after overnight coculture with EAEC. Growth competition was then assayed with EAEC cells bearing a deletion of *clpV1* or *clpV2*, two genes encoding essential components of the Sci-1 and Sci-2 T6SS respectively. While the *clpV1* mutant strain was still capable to outcompete W3110, the *clpV2* mutant strain did not inhibit W3110 growth. Our results therefore show unambiguously that the Sci-2 T6SS confers a growth advantage to EAEC by causing W3110 killing. These data were confirmed by fluorescence microscopy. EAEC *gfp*$^+$ and W3110 *mCherry*$^+$ cells were generated and a time-lapse was monitored to follow the fate of the mixed culture over a 4 hr period. *Gfp*$^+$ and *mCherry*$^+$ cells were mixed to a 10:1 ratio at a density in which bacteria form lawns under the microscope. Interestingly, few *gfp*$^+$ cells disappeared while a significant and reproducible number of *mCherry*$^+$ bacteria faded (Movie S1). When an EAEC strain deleted of the *tssE2* gene, which encodes a homolog of VCA0109 previously shown to be essential for sheath biogenesis (Basler et al., 2012), was used as predator, the number of disappearing *mCherry*$^+$ cells was significantly lower (Movie S2). W3110 *mCherry*$^+$ cells were thus killed in a Sci-2 T6SS-dependent manner. W3110 cell disappearance events were numbered by image treatment using the ImageJ software. Briefly, *mCherry*$^+$ cells present in a frame were subtracted to that of the previous frame highlighting W3110 cell fading events. We performed a quantitative image treatment using the ImageJ software to select all the individual fluorescent bacteria as single objects. All these objects were followed during the time-lapse sequence and disappearing bacteria were numbered. The numeration for a representative experiment is shown in Figure 1A. While Δ*tssE2* EAEC cells did not cause prey lysis, the wild-type (WT) EAEC strain killed the prey at constant rates. *mCherry*$^+$ cells outburst was not a rare event and ~30% of the total prey population was killed over the 4 hr coculture. Comparing the rate of *mCherry*$^+$ cells disappearing when WT or Δ*tssE2* EAEC cells were used as predators, we estimated the T6SS-independent *mCherry*$^+$ cells fading (natural or phototoxicity-induced cell death) to ~5%.

Recent studies by the Mougous laboratory suggested that T6SS-mediated killing is a cell-contact-dependent mechanism (Hood et al., 2010; Russell et al., 2011). Interestingly, close examination of disappearing *mCherry*$^+$ cells showed that >90% were in contact with at least one EAEC *gfp*$^+$ bacterium. To further test contact dependency, we performed experiments in which predators and prey were mixed to a 2:1 ratio. Time-lapse recordings showed that the vast majority of killed *mCherry*$^+$ cells were in contact with predators (Figure S1; Movie S3). The rate of disappearance of *mCherry*$^+$ cells in contact with a least one *gfp*$^+$ cell or not in contact with *gfp*$^+$ cells were quantified (Figure 1B). The data showed that the ratio was constant over the 4 hr coculture, with a lower bound estimate of 90%–95% of lysis events occurring in contact with predator *gfp*$^+$ cells. These data confirmed that prey killing is a cell-cell contact mechanism.

Recently, Basler et al. demonstrated that the T6SS assembles a phage sheath-like structure upon contact with neighboring cells (Basler et al., 2012; Basler and Mekalanos, 2012). To test whether prey killing correlates with T6SS sheath contraction, we constructed a fusion of the TssB2 protein to the superfolder green fluorescent protein (sfGFP). The TssB2-sfGFP protein behaves similarly to the *V. cholerae* fusion protein (Basler et al., 2012): (1) it assembles one to three cytoplasmic sheaths per cell, (2) the sheath structures oscillate between extended and contracted conformation with a dynamic occurring in tens of seconds, and (3) these structures are not visible in Δ*tssE2* cells

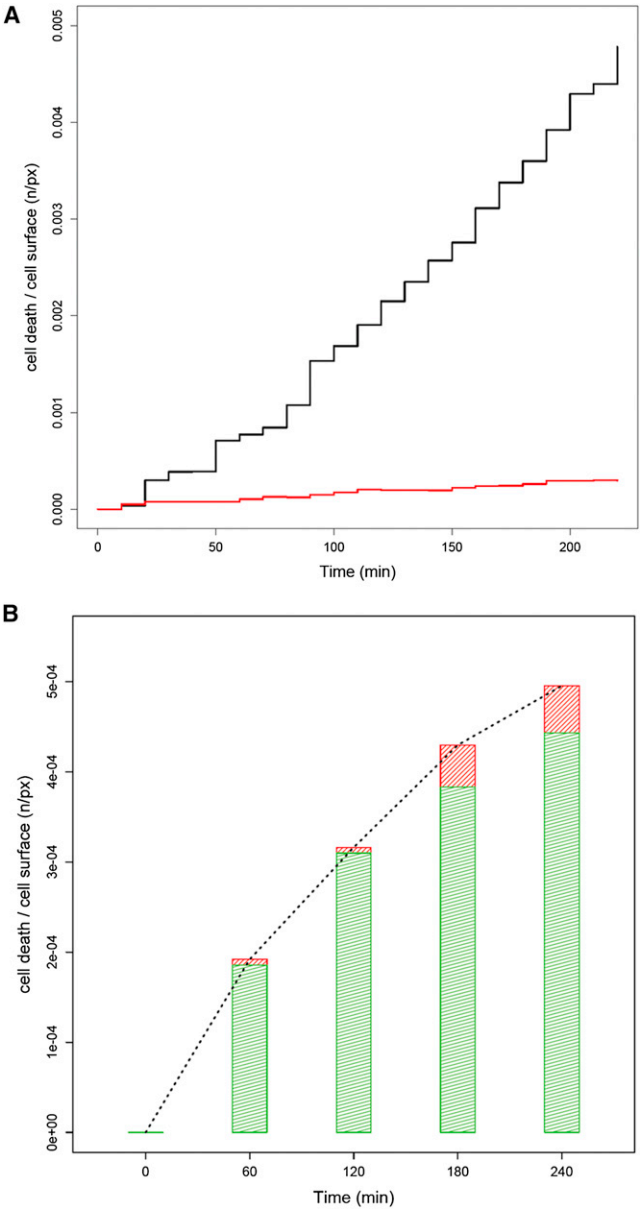

Figure 1. Predator Induces Prey Cell Lysis by a T6SS- and Cell-Contact-Dependent Mechanism

(A) The accumulated number of prey cells disappearing (n) relative to the prey cell surface (in pixel) is plotted versus time. Black line, wild-type EAEC as predator; red line, Δ*tssE2* as predator. The corresponding time-lapse recordings are shown in Movies S1 (WT) and S2 (Δ*tssE2*).

(B) The accumulated number of prey cells disappearing (n) relative to prey cell surface (in pixel) is plotted versus time (discontinuous line). For each time, the number of prey cell deaths relative to the prey cell surface is indicated (bars; green, disappearing prey cells in contact with predator cells; red, disappearing prey cells in contact with prey cells or with the medium). The corresponding time-lapse recordings are shown in Movie S3 (WT).

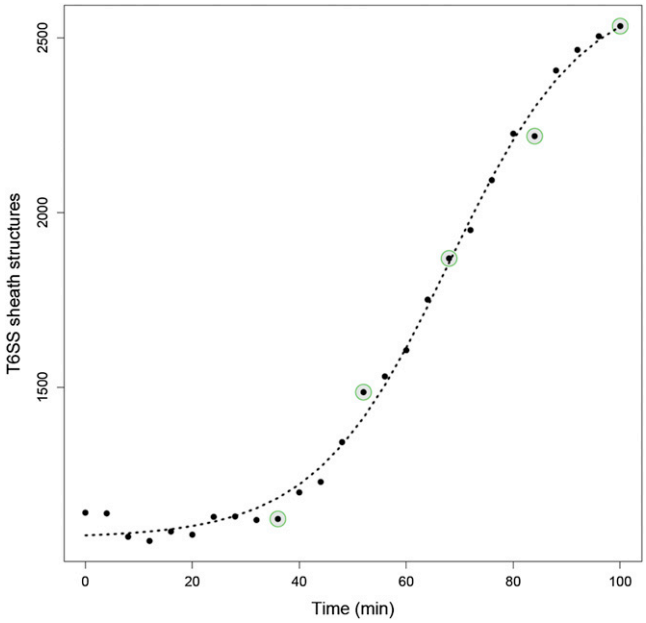

Figure 2. Propagation of T6SS Activities

The number of active T6SS sheath-like structures is plotted versus time. The corresponding time-lapse recordings are shown in Figure S3 and Movies S7 and S8. Green circles highlight the frames shown in Figure S3.

(Figure S2; Movie S4). As previously reported for *P. aeruginosa* (Basler and Mekalanos, 2012), we observed dueling between T6SS$^+$ bacteria (see below and Figure 3B). Following sheath contraction in neighboring cells, immune cells responded by increased sheath dynamics and therefore T6SS activities spread through the bacterial lawn (Movies S5 and S6). The propagation of T6SS activities through the bacterial lawn was imaged and quantified (a representative time-lapse sequence and its corresponding movies are shown in Figure S3 and Movies S7 and S8). To gain further insights into this propagation phenomenon, cells presenting an active T6SS from three independent fields were quantified and plotted against time. The resulting graph (Figure 2) perfectly fits a logistic function (Equation 1 in Experimental Procedures). This function is widely used to model bacterial growth and autocatalytic processes (Reed, 1920). The autocatalytic kinetic of sheath-like activation is consistent with cell-contact chain reaction. These data suggest that dueling contributes to the rapid propagation of T6SS activities allowing predators optimal cooperation to eliminate competing bacteria.

In coculture, we observed *mCherry*$^+$ cells fading when in contact with EAEC cells exhibiting highly dynamic sheath assembly and contraction. Interestingly, prey cell disappearance usually occurs <5 min after sheath contraction in the adjacent predator cell (Figure 3; Movies S9, S10, S11, and S12). On rare occasions, we also observed EAEC cell killing by a sister cell; however, close observation of the predated cells showed that they display diffuse TssB2-sfGFP fluorescence and therefore do not exhibit T6SS activity. This suggests that the T6SS and associated effectors/immunity genes were not expressed in these cells preventing protection against predators.

Overall, the results presented here image in vivo prey killing and constitute evidence for a correlation between sheath

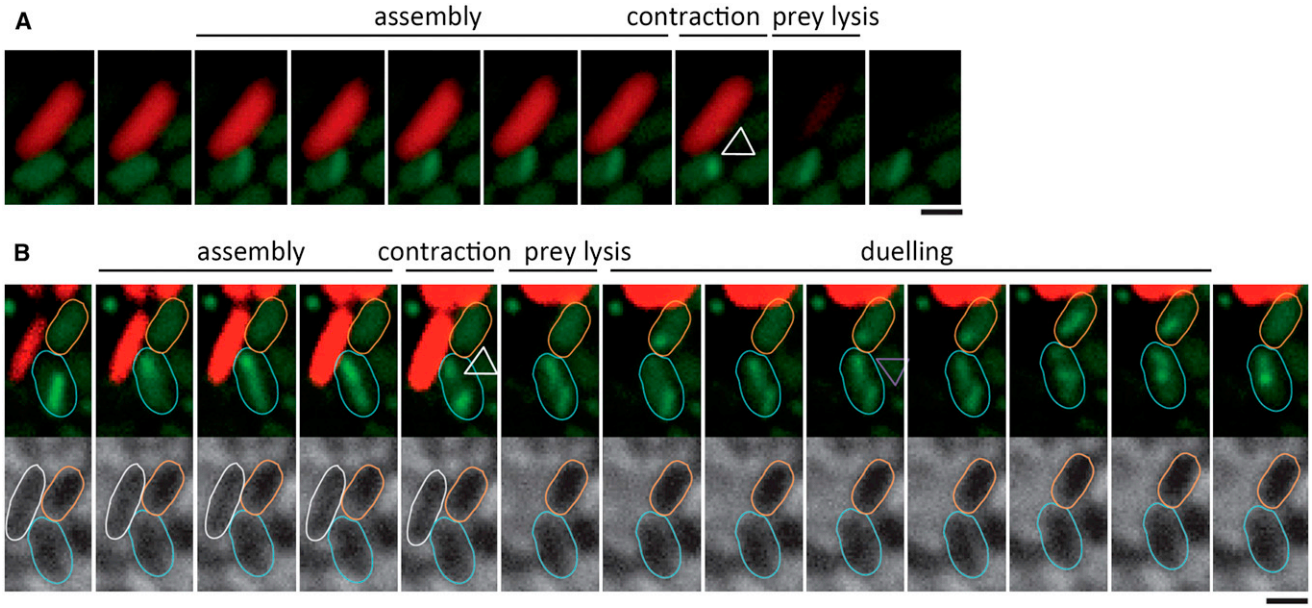

Figure 3. T6SS Sheath Contraction toward Prey Cells Causes Lysis

Fluorescence microscopy (A and B, upper panel) and phase contrast (B, lower panel) showing time-lapse competition between predator T6SS$^+$ cells producing TssB-sfGFP (GFP channel, green) and prey T6SS$^-$ cells (mCherry channel, red). The image shows the assembly and the contraction of the T6SS sheath toward a target cell and its subsequent lysis. Contracted sheath upon prey attack are indicated by white open triangles in both panels. Violet open triangle highlights a dueling event between two predator immune cells. The scale bar is 1 μm. Individual images were taken every 7.5 min. Movies S5, S6, and S7 show additional examples of dueling. Movies S9, S10, S11, and S12 show additional examples of prey cell targeting.

contraction in the T6SS$^+$ cell and death of the prey cell. These data provide strong support for a model in which translocation of T6SS effectors into the target recipient cell is achieved upon sheath contraction. We also provide data regarding the stimulation of T6SS assembly by dueling between predator cells. The propagation of sheath assembly may allow predators to outcompete competing bacteria more efficiently through cooperative efforts. Live-cell imaging of predator/prey competition will help to better understand many aspects of T6SS function such as the signal transduction mechanism underlying T6SS activation upon contact with prey cells. It will also help to understand how microbial communities are regulated and how microbes respond to the environment, collaborate, or compete.

EXPERIMENTAL PROCEDURES

Bacterial Strains, Growth Conditions, and Chemicals

Escherichia coli K12 DH5α was used for cloning procedures. The *Escherichia coli* K12 W3110 strain, the EAEC strain 17-2, and its isogenic Δ*clpV1*, Δ*clpV2*, and Δ*tssE2* derivatives were used for this study. Strains were routinely grown in lysogeny broth (LB) broth or in MEM (minimal essential medium, GIBCO) at 37°C, with aeration. Plasmids were maintained by addition of ampicillin (100 μg·ml^{-1}) or chloramphenicol (40 μg·ml^{-1}).

Bacterial Growth Competition Assay

Growth competition assays were performed using EAEC and its derivatives as predators, and the *E. coli* K12 W3110 strain as prey as described (Gueguen and Cascales, 2013). The WT *E. coli* strain W3110 bearing the kanamycin-resistant pUA66-*rrnB* plasmid (Zaslaver et al., 2006) was used as prey in the competition assay. The pUA66-*rrnb* plasmid provides a strong constitutive GFP$^+$ phenotype to *E. coli*. Cells were grown in LB at 37°C to an $OD_{600\ nm}$ of 1, adjusted to an $OD_{600\ nm}$ of 0.5, and mixed to a 4:1 ratio (predator:prey). Then, 25 μl of the mixture was spotted in triplicate onto a prewarmed dry agar plates and incubated overnight at 30°C. Bacterial spots were cut out and cells were resuspended in 1 ml of LB. Triplicates (150 μl) were transferred into wells of a black 96-well plate (Greiner), and the optical density at 600 nm and fluorescence (excitation: 485 nm; emission: 530 nm) were measured with a TECAN infinite M200 microplate reader (nine measures per mixture per experiment). The relative fluorescence was expressed as the intensity of fluorescence divided by the absorbance at 600 nm, after subtracting the values of a blank, nonfluorescent sample (the predator alone). These results are given in arbitrary units because the intensity of fluorescence was acquired with a variable gain and hence varied from one experiment to the other. The experiments were done in triplicate with identical results, and we report the results of a representative experiment. For numeration of viable cells, the bacterial suspensions recovered from the spots were serially diluted and spotted on selective kanamycin plates.

Time-Lapse Fluorescence Microscopy

Overnight cultures of *Escherichia coli* W3110 carrying plasmid pFPV-mCherry and EAEC 17.2 or 17.2Δ*tssE2* strains carrying plasmid pBAD33-TssB2–sfGFP were diluted 1:100 into MEM (GIBCO) supplemented with ampicillin or chloramphenicol, respectively, and cultivated for 3.5–4 hr to an $OD_{600\ nm}$ ~1.0. Cells were washed in PBS and mixed with a 10:1 or 2:1 ratio ($OD_{600\ nm}$ ~50). Bacterial mixtures were spotted on a thin pad of 2% agarose in PBS, covered with a coverslip, and incubated for 3 hr at 37°C before microscopy acquisition.

For each experiment, ten independent fields were manually defined with a motorized stage (Prior Scientific) and stored (X, Y, Z, PFS-offset) in our custom automation system designed for time-lapse experiments. Fluorescence and phase-contrast micrographs were captured using an automated and inverted epifluorescence microscope TE2000-E-PFS (Nikon, France), equipped with Perfect Focus System (PFS). PFS automatically maintains focus so that the point of interest within a specimen is always kept in sharp focus at all times, despite mechanical or thermal perturbations. Images were recorded with a CoolSNAP HQ 2 (Roper Scientific, Roper Scientific SARL, France) and

a 100×/1.4 DLL objective. Excitation light was emitted by a 120 W metal halide light. The sfGFP images were recorded by using the ET-GFP filter set (Chroma 49002), while the mCherry images were taken by using the ET-mCherry filter set (Chroma 49008). All fluorescence images were acquired with a minimal exposure time to minimize bleaching and phototoxicity effects. Images were collected every 7.5 or 10 min, using an exposure time of 100–200 ms for sfGFP fluorescence, 5–7 ms for mCherry fluorescence, and 5 ms for phase contrast using the Metamorph software (Molecular devices). Slight movements of the whole field during the time of the experiment were corrected by registering individual frames using StackReg and Image Stabilizer plugins for ImageJ. sfGFP and mCherry fluorescence channels were adjusted and merged using ImageJ.

Image Treatment

mCherry fluorescence sets of data were treated to monitor individual events of prey clearance. Noise and background were reduced using the "Subtract Background" (25 pixels Rolling Ball) plugin for ImageJ. In order to highlight the events of cell death, the image stacks were derivated by subtracting the n to n + 1 slides of the stack. To avoid false-positives, each event was manually controlled in the original data. The contact or noncontact events were automatically detected by a simple image processing: (1) create a mask of predator surface and dilate = Mpred; (2) create a mask of prey surface and dilate = Mprey; (3) create the contact mask by intersection Mcontact = Mpred ∩ Mprey; and (4) count the death events within the Mcontact mask. Spreading kinetics was obtained by counting the amount of sheath-like structures in each image of time-lapse recording. Sheath-like structures were identified by the "Find Maxima" process in ImageJ.

Logistic Fitting

The spreading kinetic was fitted with

$$N_t = A + \frac{K \times N0}{N0 + (K - N0)e^{-tr}}. \qquad \text{(Equation 1)}$$

Values obtained by fitting: K (carrying capacity of the system) = 1,579; N0 (initial population) = 6.961; r = −0.08; A = noise baseline = 1,069.

SUPPLEMENTAL INFORMATION

Supplemental Information includes three figures, one table, and 12 movies and can be found with this article online at http://dx.doi.org/10.1016/j.celrep.2012.11.027.

LICENSING INFORMATION

ACKNOWLEDGMENTS

We thank the members of the Cascales and Lloubès research groups and Anne Galinier for helpful comments and discussion, Adrien Ducret and members of the Mignot research group for help with fluorescence microscopy, the three anonymous reviewers for their helpful comments, and John Tulassan for encouragements. This work was supported by the Centre National de la Recherche Scientifique and a grant from the Agence Nationale de la Recherche (ANR-10-JCJC-1303-03) to E.C. Y.R.B. is a recipient of a doctoral fellowship from the French Ministère de la Recherche. Y.R.B., L.E., T.M., and E.C. designed and conceived the experiments; Y.R.B., L.E., and S.H. performed the experiments; Y.R.B., L.E., T.M., and E.C. wrote the manuscript.

Received: September 4, 2012
Revised: October 22, 2012
Accepted: November 26, 2012
Published: January 3, 2013

REFERENCES

Aschtgen, M.S., Bernard, C.S., De Bentzmann, S., Lloubès, R., and Cascales, E. (2008). SciN is an outer membrane lipoprotein required for type VI secretion in enteroaggregative *Escherichia coli*. J. Bacteriol. *190*, 7523–7531.

Basler, M., and Mekalanos, J.J. (2012). Type 6 secretion dynamics within and between bacterial cells. Science *337*, 815.

Basler, M., Pilhofer, M., Henderson, G.P., Jensen, G.J., and Mekalanos, J.J. (2012). Type VI secretion requires a dynamic contractile phage tail-like structure. Nature *483*, 182–186.

Cascales, E. (2008). The type VI secretion toolkit. EMBO Rep. *9*, 735–741.

Cascales, E., and Cambillau, C. (2012). Structural biology of type VI secretion systems. Philos. Trans. R. Soc. Lond. B Biol. Sci. *367*, 1102–1111.

Durand, E., Derrez, E., Audoly, G., Spinelli, S., Ortiz-Lombardia, M., Raoult, D., Cascales, E., and Cambillau, C. (2012). Crystal structure of the VgrG1 actin cross-linking domain of the *Vibrio cholerae* type VI secretion system. J. Biol. Chem. *287*, 38190–38199.

Gueguen, E., and Cascales, E. (2013). Promoter swapping unveils the role of the *Citrobacter rodentium* CTS1 type VI secretion system in interbacterial competition. Appl. Environ. Microbiol. *79*, 32–38.

Hood, R.D., Singh, P., Hsu, F., Güvener, T., Carl, M.A., Trinidad, R.R., Silverman, J.M., Ohlson, B.B., Hicks, K.G., Plemel, R.L., et al. (2010). A type VI secretion system of *Pseudomonas aeruginosa* targets a toxin to bacteria. Cell Host Microbe *7*, 25–37.

Jani, A.J., and Cotter, P.A. (2010). Type VI secretion: not just for pathogenesis anymore. Cell Host Microbe *8*, 2–6.

Kamada, N., Kim, Y.G., Sham, H.P., Vallance, B.A., Puente, J.L., Martens, E.C., and Núñez, G. (2012). Regulated virulence controls the ability of a pathogen to compete with the gut microbiota. Science *336*, 1325–1329.

Kanamaru, S., Leiman, P.G., Kostyuchenko, V.A., Chipman, P.R., Mesyanzhinov, V.V., Arisaka, F., and Rossmann, M.G. (2002). Structure of the cell-puncturing device of bacteriophage T4. Nature *415*, 553–557.

Kaper, J.B., Nataro, J.P., and Mobley, H.L. (2004). Pathogenic *Escherichia coli*. Nat. Rev. Microbiol. *2*, 123–140.

Leiman, P.G., Chipman, P.R., Kostyuchenko, V.A., Mesyanzhinov, V.V., and Rossmann, M.G. (2004). Three-dimensional rearrangement of proteins in the tail of bacteriophage T4 on infection of its host. Cell *118*, 419–429.

Leiman, P.G., Basler, M., Ramagopal, U.A., Bonanno, J.B., Sauder, J.M., Pukatzki, S., Burley, S.K., Almo, S.C., and Mekalanos, J.J. (2009). Type VI secretion apparatus and phage tail-associated protein complexes share a common evolutionary origin. Proc. Natl. Acad. Sci. USA *106*, 4154–4159.

Ma, A.T., McAuley, S., Pukatzki, S., and Mekalanos, J.J. (2009). Translocation of a *Vibrio cholerae* type VI secretion effector requires bacterial endocytosis by host cells. Cell Host Microbe *5*, 234–243.

MacIntyre, D.L., Miyata, S.T., Kitaoka, M., and Pukatzki, S. (2010). The *Vibrio cholerae* type VI secretion system displays antimicrobial properties. Proc. Natl. Acad. Sci. USA *107*, 19520–19524.

Mougous, J.D., Cuff, M.E., Raunser, S., Shen, A., Zhou, M., Gifford, C.A., Goodman, A.L., Joachimiak, G., Ordoñez, C.L., Lory, S., et al. (2006). A virulence locus of *Pseudomonas aeruginosa* encodes a protein secretion apparatus. Science *312*, 1526–1530.

Murdoch, S.L., Trunk, K., English, G., Fritsch, M.J., Pourkarimi, E., and Coulthurst, S.J. (2011). The opportunistic pathogen *Serratia marcescens* utilizes type VI secretion to target bacterial competitors. J. Bacteriol. *193*, 6057–6069.

Pell, L.G., Kanelis, V., Donaldson, L.W., Howell, P.L., and Davidson, A.R. (2009). The phage lambda major tail protein structure reveals a common evolution for long-tailed phages and the type VI bacterial secretion system. Proc. Natl. Acad. Sci. USA *106*, 4160–4165.

Pukatzki, S., Ma, A.T., Revel, A.T., Sturtevant, D., and Mekalanos, J.J. (2007). Type VI secretion system translocates a phage tail spike-like protein into target cells where it cross-links actin. Proc. Natl. Acad. Sci. USA *104*, 15508–15513.

Reed, H.S. (1920). The nature of the growth rate. J. Gen. Physiol. *2*, 545–561.

Russell, A.B., Hood, R.D., Bui, N.K., LeRoux, M., Vollmer, W., and Mougous, J.D. (2011). Type VI secretion delivers bacteriolytic effectors to target cells. Nature *475*, 343–347.

Schwarz, S., West, T.E., Boyer, F., Chiang, W.C., Carl, M.A., Hood, R.D., Rohmer, L., Tolker-Nielsen, T., Skerrett, S.J., and Mougous, J.D. (2010a). *Burkholderia* type VI secretion systems have distinct roles in eukaryotic and bacterial cell interactions. PLoS Pathog. *6*, e1001068.

Schwarz, S., Hood, R.D., and Mougous, J.D. (2010b). What is type VI secretion doing in all those bugs? Trends Microbiol. *18*, 531–537.

Silverman, J.M., Brunet, Y.R., Cascales, E., and Mougous, J.D. (2012). Structure and regulation of the type VI secretion system. Annu. Rev. Microbiol. *66*, 453–472.

Sperandio, V. (2012). Microbiology. Virulence or competition? Science *336*, 1238–1239.

Zaslaver, A., Bren, A., Ronen, M., Itzkovitz, S., Kikoin, I., Shavit, S., Liebermeister, W., Surette, M.G., and Alon, U. (2006). A comprehensive library of fluorescent transcriptional reporters for *Escherichia coli*. Nat. Methods *3*, 623–628.